Chapitre 3

Computing undercompressive waves with the random choice scheme. I. Nonclassical shock waves

Ce chapitre fait l'objet d'un article soumis pour publication : voir [26]

Computing undercompressive waves with the random choice scheme. I. Nonclassical shock waves

C. Chalons[1] and P.G. LeFloch[2]

Résumé

For several nonlinear hyperbolic models of interest we investigate the stability and large-time behavior of undercompressive shock waves characterized by a kinetic relation. The latter are considered as interfaces between two materials with distinct constitutive relations. In this first part we study nonclassical entropy solutions to scalar conservation laws with concave-convex flux-function and a non-genuinely nonlinear, strictly hyperbolic model of two conservation laws arising in nonlinear elastodynamics. We use Glimm's random choice scheme but we replace the classical Riemann solver with the *nonclassical* one described recently in [88, 95]. Our numerical experiments demonstrate the great interest of using the random choice scheme for computing nonclassical shock waves which are known to be very sensitive to dissipation and dispersion mechanisms. In this paper, we study carefully various issues related to nonclassical shocks and their stability and instability under perturbations.

3.1 Introduction

We are interested in computing weak solutions of the initial-value problem for one-dimensional, nonlinear systems of conservation laws of the form

$$\partial_t u + \partial_x f(u) = 0, \quad u(x,t) \in I\!R^N,\, x \in I\!R,\, t > 0, \tag{3.1}$$

$$u(x,0) = u_0(x), \qquad x \in I\!R. \tag{3.2}$$

Such systems arise in a broad spectrum of problems in compressible fluid dynamics, nonlinear elastodynamics, etc. Due to the nonlinearity $f : I\!R^N \to I\!R^N$, solutions are generally discontinuous and it is well-known that weak solutions (in the integral sense) are not uniquely determined by their initial data $u_0 : I\!R \to I\!R^N$, and must be constrained by an *entropy inequality* of the form

$$\partial_t U(u) + \partial_x F(u) \le 0 \tag{3.3}$$

in the weak sense, where (U, F) denotes an entropy-entropy flux pair for the system (3.1), satisfying by definition $DF^T = DU^T Df$. Here, we will focus on solutions containing *undercompressible shock waves:* the number of characteristics (wave modes) impinging on the discontinuity is less than what is usually required for the linearized stability. Undercompressive waves turn out to be not uniquely determined by (3.3). However, under some assumptions to be specified in several examples below, the uniqueness of the *entropy solution* of the problem (3.1)-(3.3) is ensured when a *kinetic*

1. O.N.E.R.A., B.P. 72, 29 avenue de la Division Leclerc, 92322 Châtillon Cedex, France. E-mail: chalons@onera.fr.

2. Centre de Mathématiques Appliquées & Centre National de la Recherche Scientifique, U.M.R. 7641, Ecole Polytechnique, 91128 Palaiseau Cedex, France. E-mail: lefloch@cmap.polytechnique.fr.

relation is added along each undercompressive discontinuity connecting a left-hand state u_- to a right-hand state u_+:

$$u_+ = \varphi^\flat(u_-). \tag{3.4}$$

The *kinetic function* $\varphi^\flat : I\!R^N \to I\!R^N$ is a Lipschitz continuous mapping satisfying the basic conditions

$$-\lambda^\flat(u_-)\,(\varphi^\flat(u_-) - u_-) + f(\varphi^\flat(u_-)) - f(u_-) = 0 \tag{3.5}$$

and

$$-\lambda^\flat(u_-)\,(U(\varphi^\flat(u_-)) - U(u_-)) + F(\varphi^\flat(u_-)) - F(u_-) \leq 0, \tag{3.6}$$

where $\lambda^\flat(u_-)$ denotes the speed of propagation. The nonclassical shocks are also refer as *phase transition* or *interfaces*. For a complete discussion of the notion of kinetic relation we refer to the recent monograph [89] and the references therein.

Our general aim is to investigate numerically the stability and large-time behavior of undercompressive waves using, as a tool, Glimm's random choice scheme [55]. In the present paper, we focus attention on *nonclassical shocks* of strictly hyperbolic systems which fail to be globally genuinely nonlinear in the sense of Lax. That is, the Jacobian matrix $Df(u)$ admits real and distinct eigenvalues $\lambda_j(u)$ and independent eigenvectors $r_j(u)$ $(1 \leq j \leq N)$ and for one wave family at least the product $\nabla\lambda_j(u) \cdot r_j(u)$ does not keep a constant sign. Specifically, we consider the scalar conservation law with cubic flux-function (Section 3.2) and an hyperbolic model arising in nonlinear elastodynamics (Section 3.3). In the second part [27] we will study phase boundaries of an hyperbolic-elliptic model arising in phase dynamics.

Let us recall some basic features of the random choice method. Glimm's scheme [55, 100, 30] is based on an equidistributed sequence $(a_n)_{n=1,2,\cdots}$ of values in the interval $(0,1)$ satisfying, by definition, for each interal $J \subset (0,1)$

$$\frac{1}{m}\,\mathrm{card}\{n\,/1 \leq n \leq m \ \text{ and } \ a_n \in J\} \to \mathrm{meas}(J)$$

as $m \to \infty$. The scheme is based on solving *Riemann problems* corresponding to the piecewise constant initial data:

$$u_0(x) = \begin{cases} u_L, & x < 0, \\ u_R, & x > 0, \end{cases} \tag{3.7}$$

where u_L and u_R are constant states. The Riemann solution has a rather simple form: explicitely, it is made of several shock waves and rarefaction waves separated by constant states. Glimm's scheme proceeds as follows. First, the initial data u_0 in (3.2) is replaced by a piecewise constant approximation $u_0^{\Delta x}$ where $\Delta x > 0$ represents the constant mesh size of a regular mesh $x_k = k\,\Delta x$ for $k = \cdots, -1, 0, 1, \cdots$ At each initial discontinuity a Riemann problem is solved locally, using a classical or a nonclassical Riemann solver. (Such solvers are derived in [88].) At some sufficiently small time Δt satisfying the stability condition

$$\Delta t\ \sup|\lambda_j(u)| < \frac{\Delta x}{2}, \tag{3.8}$$

a value is picked up "randomly" within each local Riemann solutions. This provides us with the new approximation at time Δt. The construction is continued inductively in time until the approximation $u^{\Delta x,\Delta t} = u^{\Delta x,\Delta t}(x,t)$ is determined for all times.

Throughout the present paper, following a proposal by Collela [30] we use van der Corput random sequence defined by

$$a_n = \sum_{k=0}^{m} i_k 2^{-(k+1)},$$

where $n = \sum_{k=0}^{m} i_k 2^k$, $i_k = 0,1$, denotes the binary expansion of the integers $n = 1, 2, \ldots$. The first few elements of this sequence are

$$\begin{array}{llll} 1 = 1_2, & a_1 = 0.5, & 2 = 10_2, & a_2 = 0.25, \\ 3 = 11_2, & a_3 = 0.75, & 4 = 100_2, & a_4 = 0.125, \\ 5 = 101_2, & a_5 = 0.625, & 6 = 110_2, & a_6 = 0.375, \\ 7 = 111_2, & a_7 = 0.875, & 8 = 1000_2, & a_8 = 0.0625. \end{array}$$

This sequence is well distributed within the interval. For instance one can prove that

$$\begin{array}{ll} a_i < 0.5, & i \text{ even}, \\ a_i > 0.5, & i \text{ odd}. \end{array}$$

Excellent numerical results in the smooth parts of the solution are obtained with this sequence, as we will illustrate below (Test 1).

3.2 Conservation Law with Cubic Flux

To begin with, we consider the nonlinear conservation law

$$\partial_t u + \partial_x u^3 = 0, \quad u(x,t) \in I\!R, \tag{3.9}$$

which is the simplest example of a nonlinear hyperbolic equation which fails to be globally genuinely nonlinear. Following [69, 89] we consider solutions satisfying the conservation law (3.9) in the integral sense, the initial condition

$$u(x,0) = u_0(x), \qquad x \in I\!R, \tag{3.10}$$

the entropy inequality

$$\partial_t u^2 + \frac{3}{2}\,\partial_x u^4 \le 0 \tag{3.11}$$

in the integral sense and (for definiteness in our numerical investigations) a kinetic function in the form

$$\varphi^\flat(u) = -\beta\, u, \quad \beta \in [1/2, 1). \tag{3.12}$$

The parameter β is a measure of "how far the solution" is from the classical regime. Precisely, as $\beta \to 1/2$, the Riemann solution converges to the classical entropy solution selected by Oleinik entropy inequalities. The choice $\beta = 1$ is not truly allowed in the general theory of [88], but is a limiting case, associated with the "maximal kinetic relation": The correponding shock waves have zero-entropy dissipation and achieve the largest propagation speed among all admissible nonclassical shocks.

Observe that (3.12) satisfies the standard assumption made on kinetic functions in [89]:

$$\begin{aligned} -u < \varphi^{\flat}(u) \le -u/2, &\quad u > 0, \\ -u/2 \le \varphi^{\flat}(u) < -u, &\quad u < 0. \end{aligned}$$

We also set

$$\varphi^{\sharp}(u) = -u - \varphi^{\flat}(u).$$

Given constant states u_L and u_R, the *nonclassical Riemann solver* associated with (3.9)-(3.12) and the initial data

$$u_0(x) = \begin{cases} u_L, & x < 0, \\ u_R, & x > 0, \end{cases}$$

is given as follows, assuming for definiteness that $u_L > 0$:

(1) If $u_R \ge u_L$, the solution is a rarefaction wave connecting u_L to u_R.
(2) If $u_R \in [\varphi^{\sharp}(u_L), u_L)$, the solution is a classical shock wave connecting u_L to u_R.
(3) If $u_R \in (\varphi^{\flat}(u_L), \varphi^{\sharp}(u_L))$, the solution contains a nonclassical shock connecting u_L to $\varphi^{\flat}(u_L)$, followed by a classical shock connecting $\varphi^{\flat}(u_L)$ to u_R.
(4) If $u_R \le \varphi^{\flat}(u_L)$, the solution contains a nonclassical shock connecting u_L to $\varphi^{\flat}(u_L)$, followed by a rarefaction connecting $\varphi^{\flat}(u_L)$ to u_R.

Test 1 : Van der Corput sequence

We start by comparing the efficiency of van der Corput sequence versus an "arbitrary" random sequence. Consider the Riemann data

$$u_0(x) = \begin{cases} 2, & x < 0, \\ 4, & x > 0. \end{cases}$$

The solution is made of a single rarefaction wave and the kinetic function is here irrelevant. The mesh contains 300 points and the solution is plotted on Figure 3.1 at the time $t = 0.007$. We observe that van der corput sequence gives much more accurate and regular results than an arbitrary random sequence.

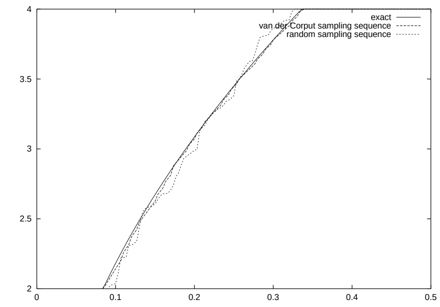

FIG. 3.1 – *Two random sequences*

Test 2 : The Riemann solver

Next, we display the four qualitative behaviors of the Riemann solution for the problem (3.9)-(3.12), with

$$u_0(x) = \begin{cases} u_l, & x < -0.375, \\ u_r, & x > -0.375, \end{cases}$$

and the parameter value $\beta = 2/3$. The mesh contains 300 points and numerical solutions are plotted on Figures 3.2 and 3.3. We observe that the numerical solutions fully agree with the above nonclassical Riemann solver.

• Figure 3.2 (a): *A single classical shock wave.* We plot here the numerical solution at the time $t = 0.05$, corresponding to the data $u_l = 2$ and $u_r = 1$.

• Figure 3.2 (b): *A single rarefaction wave.* We plot the solution obtained with $u_l = 1$ and $u_r = 2$, at the time $t = 0.05$.

• Figure 3.3 (c): *A nonclassical shock wave followed by a classical shock wave.* We plot the numerical solution at the time $t = 0.6$, corresponding to the Riemann data $u_l = 1$ and $u_r = -0.4$.

• Figure 3.3 (d): *A nonclassical shock wave followed by a rarefaction wave.* We plot the numerical solution at the time $t = 0.05$, corresponding to $u_l = 1$ and $u_r = -2$.

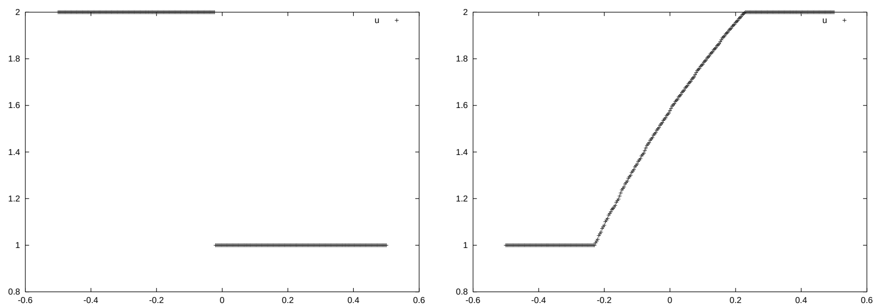

FIG. 3.2 – *(a) and (b) Typical solutions : single classical wave*

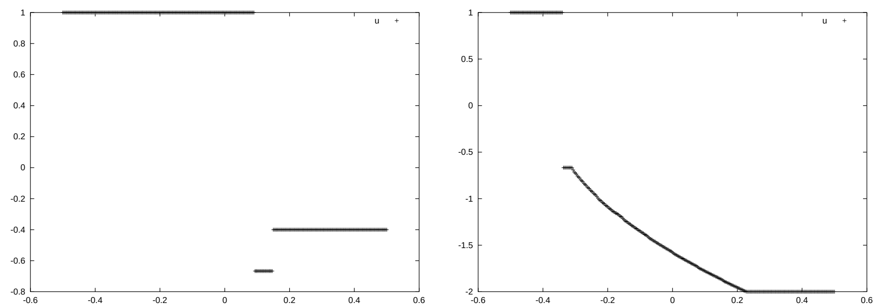

FIG. 3.3 – *(c) and (d) Typical solutions : classical wave and nonclassical wave*

Observe that shock waves are represented by sharp discontinuities which is a main feature of the random choice scheme: all values taken by the numerical solutions are actual values taken by the exact solutions. The location of the discontinuities however depend on the random sequence. By constrast, finite differences schemes generate intermediate points within propagating discontinuity and a discrete numerical shock profile.

Test 3 : Splitting of shock waves

We present three related approaches illustrating an important numerical difficulty encountered with nonclassical shock waves: the nonclassical Riemann solver depend continuously upon its end states in the integral norm but *not* in the pointwise sense. Because of this lack of continuity, some sort of "spikes" are sometimes observed in the numerical solution. The Riemann problem associated with

$$u_0(x) = \begin{cases} u_L, & x < -0.375, \\ \varphi^\sharp(u_L), & x > -0.375, \end{cases}$$

can be solved with a single classical shock wave.

• Figure 3.4: *Small perturbations of a classical shock.* If we perturb the above initial data by an arbitrarily small amount $\epsilon > 0$, specifically

$$u_0^\epsilon(x) = \begin{cases} u_L, & x < -0.375, \\ \varphi^\sharp(u_L) - \epsilon, & x > -0.375, \end{cases}$$

the solution now contains a *two-wave, non-monotone pattern,* precisely a nonclassical shock connecting u_L to $\varphi^\flat(u_L)$ followed with a classical shock connecting $\varphi^\flat(u_L)$ to $\varphi^\sharp(u_L) - \epsilon$.

On Figure 3.4, using $\epsilon = 0.01$, $\epsilon = 0.05$, and $\epsilon = 0.1$ successively, we plotted the numerical Riemann solution, for a mesh containing 300 points, at the time $t = 0.18$, and with $\beta = 2/3$. We observe that, as ϵ diminishes, the wave speeds of the two shocks become closer and the solution exhibits a *spike,* while the intermediate value is determined *exactly* by Glimm's scheme. This feature is *not* shared by finite differences scheme and the presence of spikes may be an important source of error in numerical computations performed with finite differences schemes.

• Figure 3.5: *Interaction of a classical shock and a rarefaction.* Second, consider the initial data

$$u_0(x) = \begin{cases} u_L, & x < -0.40, \\ \varphi^\sharp(u_L) + \epsilon, & -0.40 < x < -0.38, \\ \varphi^\sharp(u_L) - \epsilon, & x > -0.38. \end{cases}$$

The solution contains, for small times, a classical shock wave plus a rarefaction wave (with arbitrary small strength) which interact in finite time and generate a nonclassical shock. In Figure 3.5, for $\epsilon = 0.01$, $\epsilon = 0.05$, and $\epsilon = 0.1$ successively, we plot the numerical solution obtained with 300 points, at the time $t = 0.2$ with $\beta = 2/3$. We note that the total variation of the solution *after* the interaction is much *greater* than the total variation of the initial data:

$$TV(u(t)) > TV(u_0).$$

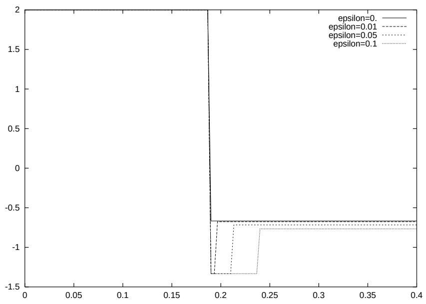

FIG. 3.4 – *Small perturbations of a classical shock*

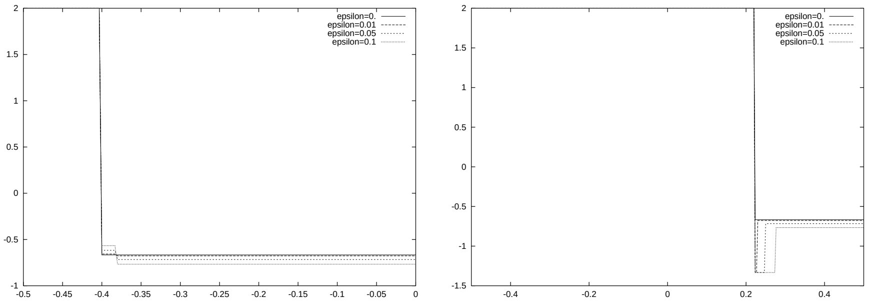

FIG. 3.5 – *Interaction of two classical shocks ($t = 0$ and $t = 0.2$)*

• Figures 3.6-3.7: *Large perturbations.*

This last test is different in nature. We demonstrate here that nonclassical shocks (as well as classical shocks) are stable under large perturbations, in the following sense: when a large perturbation is added at the initial time within a classical shock wave (Figure 3.6) or a nonclassical shock wave (Figure 3.7), the solution *converges asymptotically in time* to the unperturbed initial wave. More precisely, this is true up to a possible *shift* in the location of the discontinuity. In the numerical experiments, the amplitude of the perturbation lies between -0.42 et -0.35. At the time under consideration in Figure 3.6, the unperturbed shock should be located at the point -0.42.

Test 4 : Periodic data

We begin with the initial condition

$$u_0(x) = -0.5 + \sum_{i=0}^{4} \cos(5ix), \quad x \in [-0.5, 0.5]$$

with periodic boundary conditions

$$u(-0.5, t) = u(0.5, t).$$

The averaged of the solution over one period is constant and in our experimentrs equals about 0.61826856. Throughout we use a mesh containing 300 points.

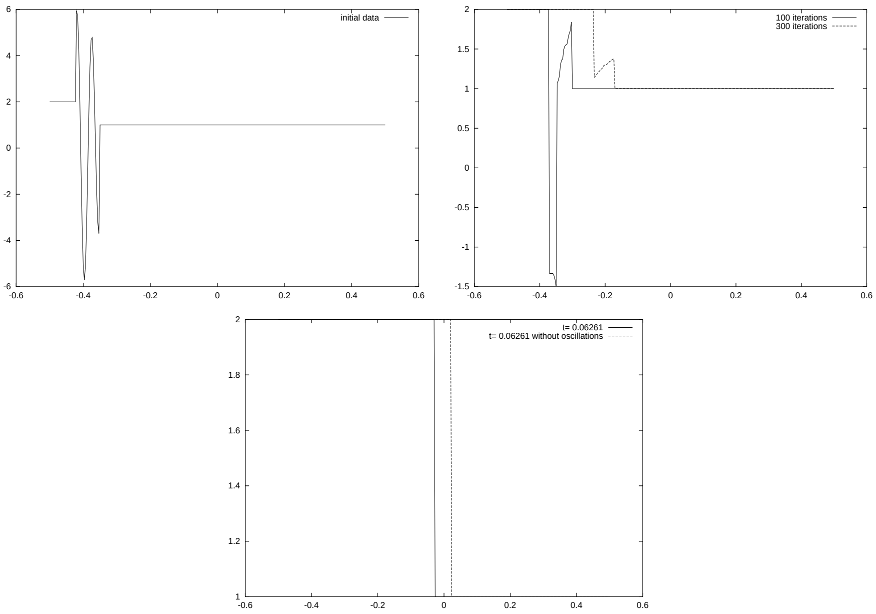

FIG. 3.6 – *Large perturbations (classical shock)*

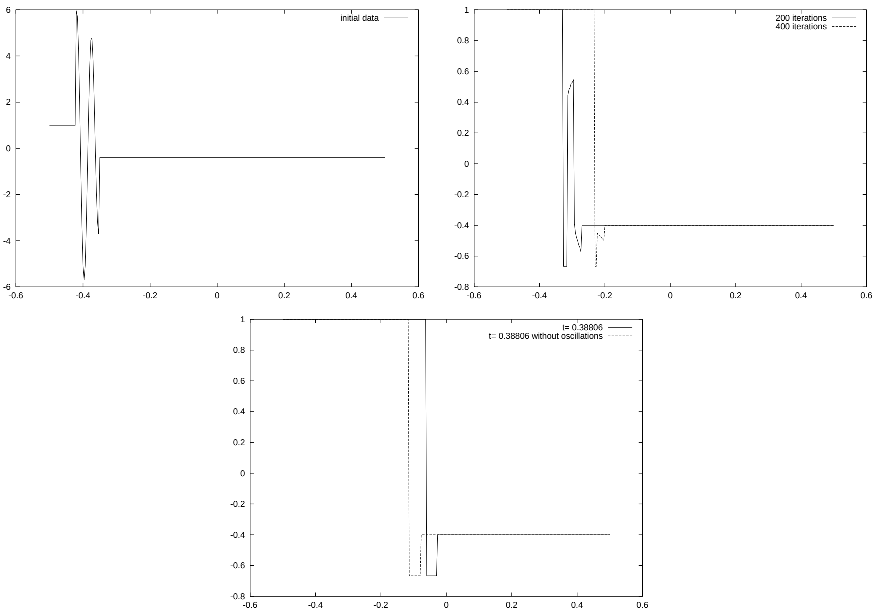

FIG. 3.7 – *Large perturbations (nonclassical shock + classical shock)*

• Figure 3.8: *Classical Riemann solution with positive average.* To begin with, we use the classical kinetic function corresponding to $\beta = 1/2$. On Figure 3.8, we see that the number of phase transitions is *decreasing* in time and that the numerical solution converges to a constant value. In the last figure we recognize the so-called *N-wave* which is well-known for scalar conservation laws with convex flux. Since the average value is positive, for sufficiently large times the solution takes positive values only, and the convex part of the flux only is relevant.

• Figure 3.9: *Nonclassical Riemann solution with positive average.* We use now $\beta = 2/3$. We observe that the number of phase transitions is still *decreasing* and that the solution converges to a constant state. Again, we recognize an *N-wave.* Since the average value is positive, for sufficiently large times the solution takes positive values only, the convex part of the flux only is relevant and the nonclassical solver coincides with the classical solver in this region, and the solution is eventually entirely classical. Observe also that Figures 3.8 and 3.9 are qualitatively similar, the maximal value in the asymptotic nonclassical solution being larger then the one in the classical solution.

• Figure 3.10: *Maximal nonclassical Riemann solution with positive average.* Finally, we use $\beta = 1$ and observe that the numerical solution no longer converges to a constant state. Instead, the number of phase transitions remains *constant* and the solution converges to a piecewise constant function made of *several phase transitions* with coinciding propagation speeds.

• Figure 3.11-3.12: *The case $\beta = 1 - \epsilon$ with ϵ small.* Taking $\epsilon = 0.01$, we observe that the qualitative behavior of the solution is quite analogous to Figure 3.9. However, the convergence is *very slow,* and there is a transient regime during which the solution may appear to *behave like* the one in Figure 3.10. The number of phase transitions is *very slowly decreasing* but the solution does eventually converge to the average value of the initial data.

• Figure 3.13: *Classical Riemann solution with zero average.* In the remaining tests in this series, we consider the periodic initial condition with period 1/2:

$$u_0(x) = \cos(4\pi x),$$

which has *zero average.* Throughout, the mesh contains 300 points and to begin with we take $\beta = 1/2$. We observe here that the number of phase transitions is *decreasing* and that the solution *converges to zero* in a pointwise sense. More precisely, a new feature must be pointed out: there is a transient regime during which the solution exhibits what we will call a *"double N-wave pattern",* which is somewhat made of two standard well-known N-wave profiles with opposite monotonicity. Notice that the period 1/2 is eventually lost as the numerical solution converges eventually to a standard N-wave profile. See also Test 5 below for further mesh refinements.

• Figure 3.14: *Nonclassical Riemann solution with zero average.* Next, we use $\beta = 2/3$. The number of phase transitions is *decreasing* and the solution converges

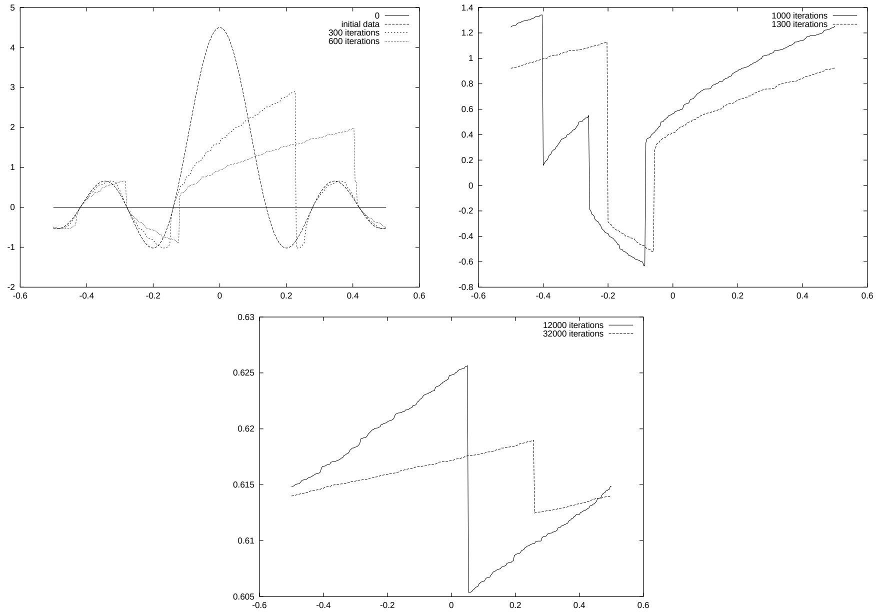

FIG. 3.8 – *Classical Riemann solution with positive average*

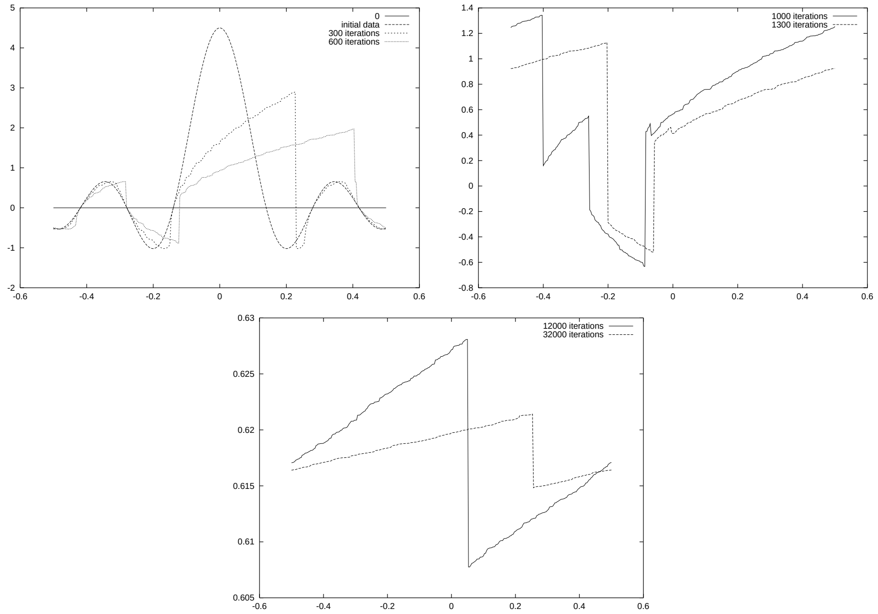

FIG. 3.9 – *Nonclassical Riemann solution with positive average*

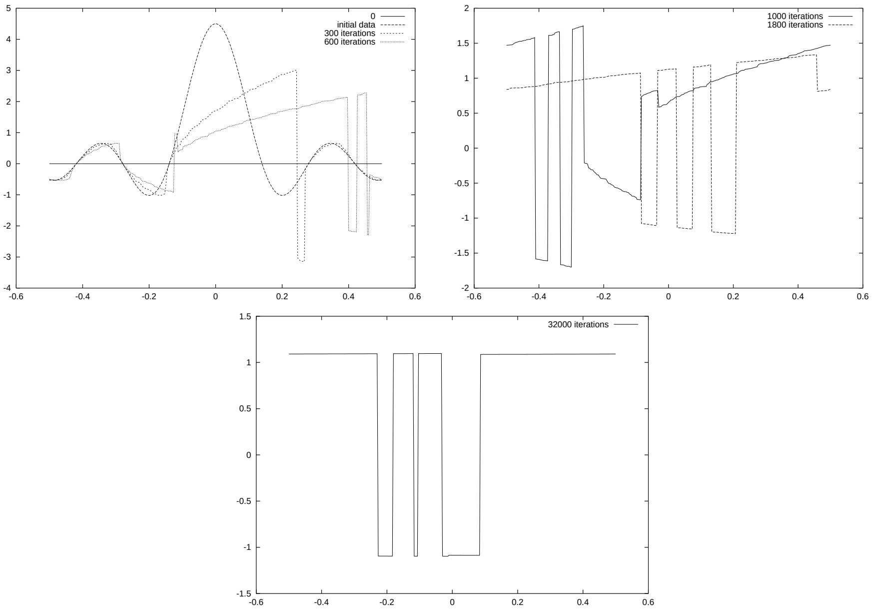

FIG. 3.10 – *Maximal nonclassical Riemann solution with positive average*

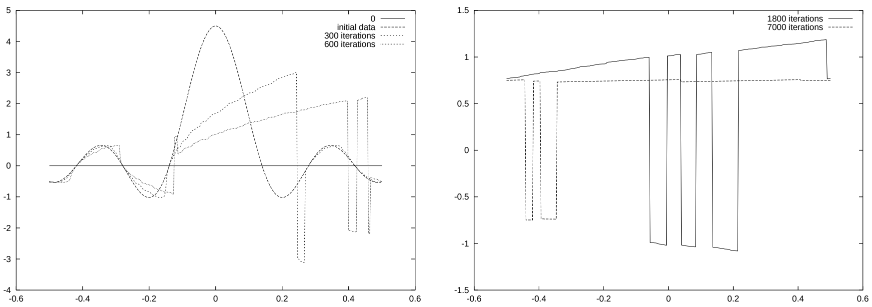

FIG. 3.11 – *The case* $\beta = 1 - \epsilon$

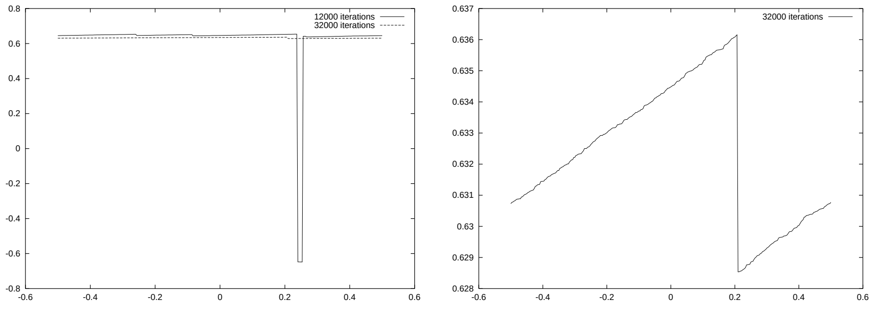

FIG. 3.12 – *The case* $\beta = 1 - \epsilon$

to zero. Again, we observe a double N-wave which eventually disappears and get transformed into a more familiar single N-wave.

• Figure 3.15: *Maximal nonclassical Riemann solution with zero average.* Finally, we use $\beta = 1$ and notice that the number of phase transitions is now *constant* in time. The numerical solution converges to a function made of several phase transitions with coinciding propagation speeds.

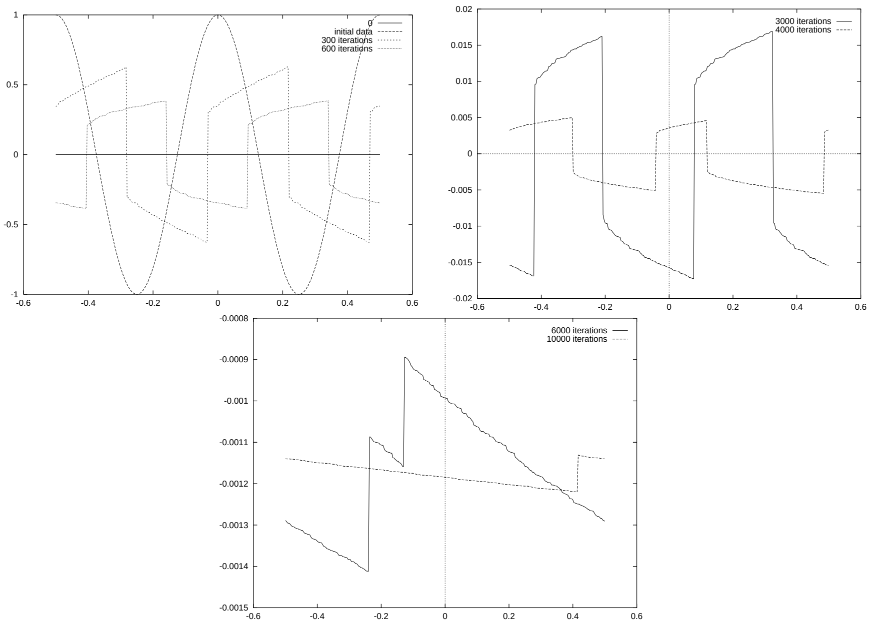

FIG. 3.13 – *Classical Riemann solution with zero average*

Test 5 : Mesh refinements

Two mesh refinement experiments are described here. First, using $\beta = 2/3$ and

$$u_0(x) = \begin{cases} 3, & x < -0.375, \\ -3, & x > -0.375, \end{cases}$$

on Figure 3.16 we plotted the numerical solution corresponding to finer and finer mesh lengths, at the time $t = 0.023$. As expected, the numerical solution approaches the exact solution determined by our nonclassical Riemann solver. This illustrates the convergence property of the random choice scheme to nonclassical entropy solutions.

Second, we plotted on Figure 3.17 the solution with the initial periodic data

$$u_0(x) = \cos(4\pi\, x),$$

for several mesh lengths. As expected, we observe that the numerical solution gets closer and closer to the exact solution (that is 0) pointwisely as the mesh is refined. We do observe a convergence to the double N-wave profile discovered in Test 4.

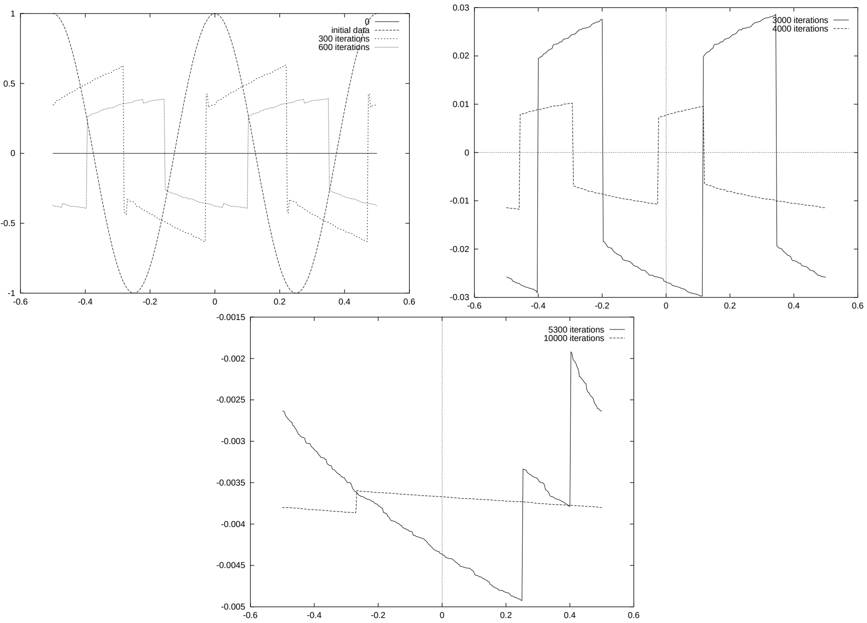

FIG. 3.14 – *Nonclassical Riemann solution with zero average*

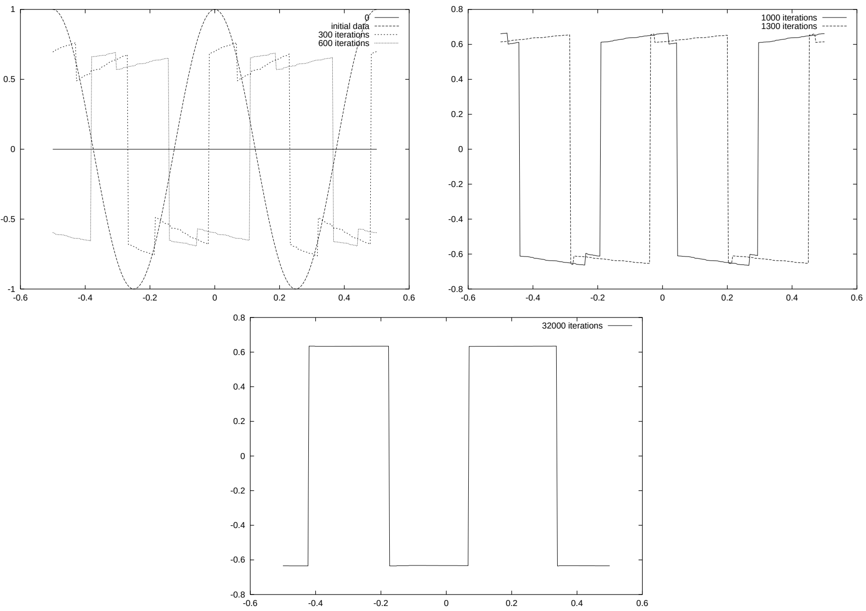

FIG. 3.15 – *Maximal nonclassical Riemann solution with zero average*

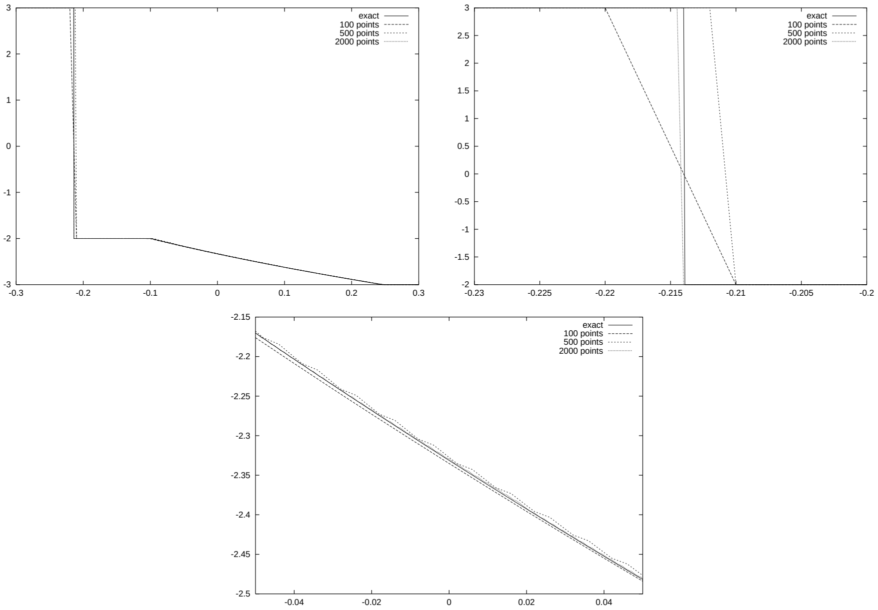

Fig. 3.16 – *Mesh refinement (global solution and zooms)*

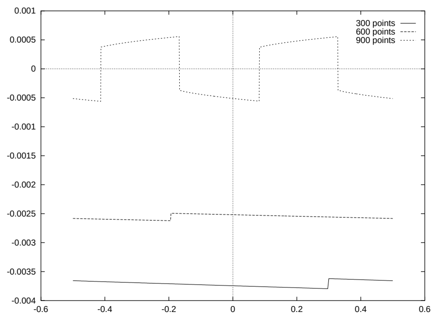

Fig. 3.17 – *Mesh refinement (periodic data)*

3.3 Hyperbolic Model of Nonlinear Elastodynamics

We turn to the following model of two conservation laws for the mass and momentum of some nonlinear material, with prescribed initial data (v_0, w_0),

$$\begin{aligned} &\partial_t v - \partial_x \sigma(w) = 0, \qquad x \in I\!R,\ t > 0, \\ &\partial_t w - \partial_x v = 0, \\ &(v(x,0), w(x,0)) = (v_0(x), w_0(x)), \qquad x \in I\!R, \end{aligned} \tag{3.13}$$

where v and w represent the velocity and the deformation gradient of the material, respectively. The strain-stress function σ is taken to be

$$\sigma(w) = w^3 + m\, w, \tag{3.14}$$

with $m = 2$ for the numerical experiments below (excepted when mentioned otherwise). The Cauchy problem (3.13) is supplemented with the following *kinetic function* for each undercompressive nonclassical shock

$$\varphi^\beta(w) = -\beta\, w, \tag{3.15}$$

where $\beta \in [1/2, 1)$ is a parameter. We refer to [95] for a detailled discussion of the nonclassical Riemann solver corresponding to this problem. We simply recall here that when $\beta = 1/2$ the nonclassical Riemann solver actually coincides with the classical solver characterized, for instance, by Liu entropy criterion. When $\beta > 1/2$, the Riemann solution may contain shock waves which violate Liu criterion, are undercompressive, and satisfy the *kinetic relation*

$$\begin{aligned} w_+ &= \varphi^\beta(w_-) \quad \text{for shock with positive speed,} \\ w_- &= \varphi^\beta(w_+) \quad \text{for shock with negative speed.} \end{aligned} \tag{3.16}$$

As was noticed with scalar conservation laws, the "maximal kinetic relation" corresponding to $\beta = 1$ is not truly allowed in the general theory of [88] but can be regarded as an interesting limiting case. The corresponding shock waves have zero-entropy dissipation and achieve the largest propagation speed (in modulus) among all admissible nonclassical shocks.

Test 6 : Splitting of shock waves

• Figure 3.18: *Small perturbations of a classical shock.* We consider the Riemann initial data

$$(v_0(x), w_0(x)) = \begin{cases} (1, 1+\epsilon), & x < 0.5, \\ (-11, -3), & x > 0.5, \end{cases}$$

and we plot the corresponding numerical solution for several values of ϵ. When $\epsilon = 0$, the exact solution of the Riemann problem is a single classical shock. We see that the structure for arbitrary small values ϵ is entirely different from the one with $\epsilon = 0$. In particular, the L^∞-norm of the solution is *not continuous* as $\epsilon \to 0$. We use a mesh with 600 points by unit interval, $t = 0.4$, and $\beta = 2/3$.

• Figures 3.19-3.20: *Interaction of two classical waves.* As in the scalar case, two incoming waves (of the same family) may interact and can generate a nonclassical

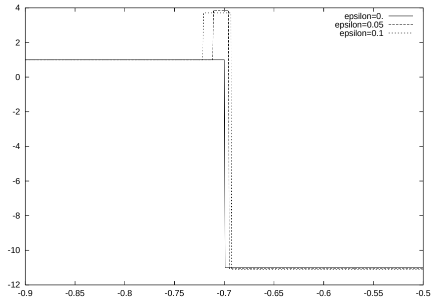

FIG. 3.18 – *Small perturbations of a classical shock (v and w components)*

shock wave. The total variation of the solution increases at the interaction and the w-component becomes non-monotone after the interaction. Of course, it is well-known that, for hyperbolic systems of conservation laws, the total variation may increase at interactions; however, the increase here is not of the order of the product of the strengths of the incoming waves. Specifically, we consider the initial data

$$(v_0(x), w_0(x)) = \begin{cases} (1, 1.2), & x < -0.1, \\ (-1.72814176, -0.337385342), & -0.1 < x < 0.1, \\ (-11, -3), & x > 0.1, \end{cases}$$

and we plot the solutions after various iteration numbers. We use a mesh with 300 points per unit interval.

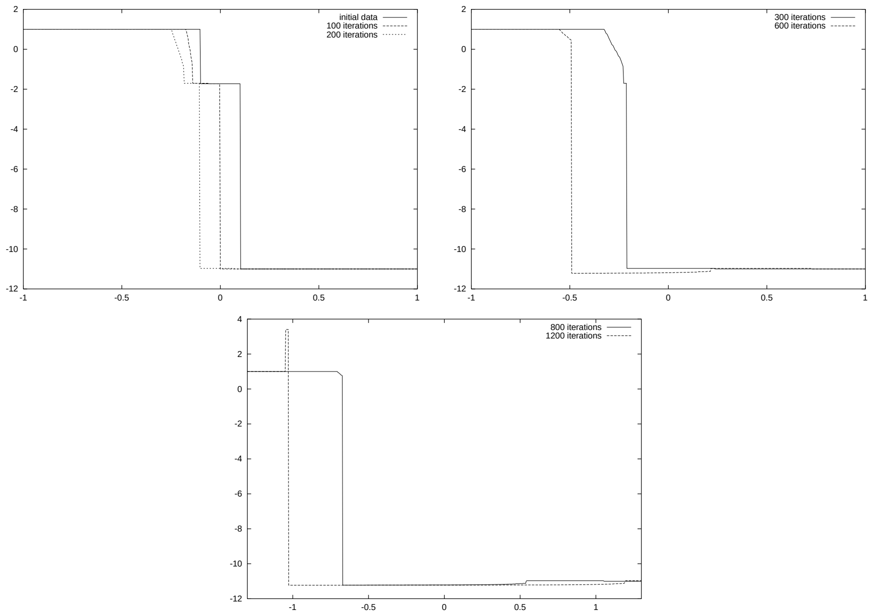

FIG. 3.19 – *Interaction of two classical shocks (v component)*

• Figures 3.21-3.22: *Large perturbations.* Finally, we observe that the nonclassical Riemann solver (as well as the classical one) is stable under possibly large pertur-

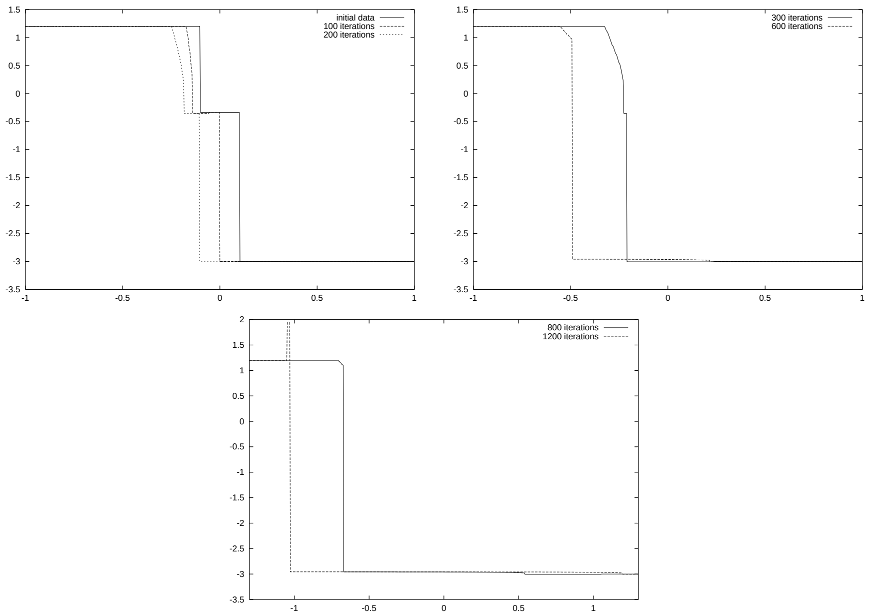

FIG. 3.20 – *Interaction of two classical shocks (w component)*

bations. Oscillations ranging between -0.03 and 0 are introduced in a given initial data. The discontinuity is located at 0 when no oscillations are present. The left-hand state is taken to be $(v_L, w_L) = (0, 1)$ and the right-hand state $(v_R, w_R) = (-6.71190015066, -2)$. We use a mesh containing 200 points per unit interval. We observe that the unperturbed profile is recovered asymptotically in time, but the position of the discontinuity is shifted.

Test 7 : Periodic data

As in the scalar case, we now study the asymptotic behavior of the solutions for several kinetic functions. We use the stress-function given by (3.14), but with now $m = 0.05$, and a mesh containing 1000 points.

• Figures 3.23-3.28: *The classical case.* First, we consider the case $\beta = 1/2$ and the following periodic initial data

$$(v_0(x), w_0(x)) = \begin{cases} (0, 0.4), & x < x_0, \\ (0, -0.2), & x_0 < x < x_1, \\ (0, 0.4), & x > x_1, \end{cases} \tag{3.17}$$

where x_0 and x_1 will be specified shortly. Each of the following computations is performed over the unit interval $[-0.5; 0.5]$ with periodic boundary conditions.

First, we choose $x_0 = 0$ and $x_1 = 0.3$ so that the corresponding average $\overline{w}_0$ of w_0 is positive, precisely $\overline{w}_0 = 0.22$. The components v and w are plotted on Figures 3.23 and 3.24, while Figure 3.25 shows the two Riemann invariants

$$v - \int^w \sqrt{\sigma'(x)}\, dx \quad \text{and} \quad v + \int^w \sqrt{\sigma'(x)}\, dx$$

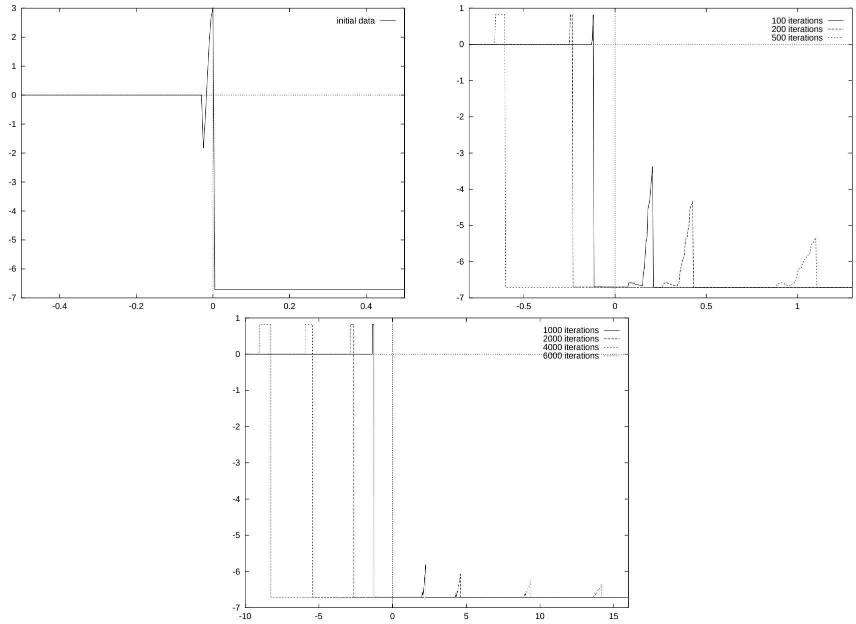

FIG. 3.21 – *Large perturbations (v component)*

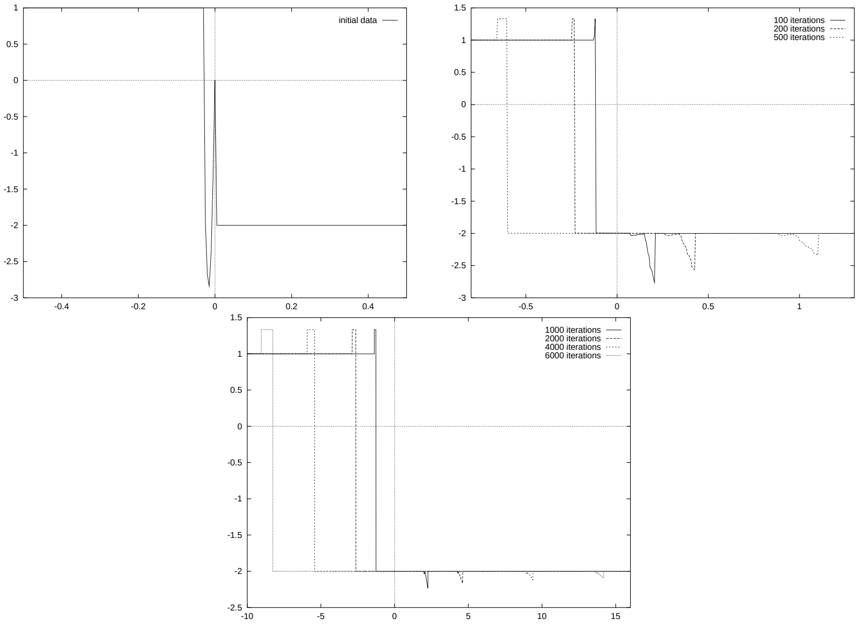

FIG. 3.22 – *Large perturbations (w component)*

after linearization near the average value $\overline{w}_0$, that is,

$$v - \sqrt{\sigma'(\overline{w}_0)}\, w \quad \text{and} \quad v + \sqrt{\sigma'(\overline{w}_0)}\, w.$$

We observe that, as the time evolves, these variables exhibit *two standard N-waves,* propagating at speed with opposite signs.

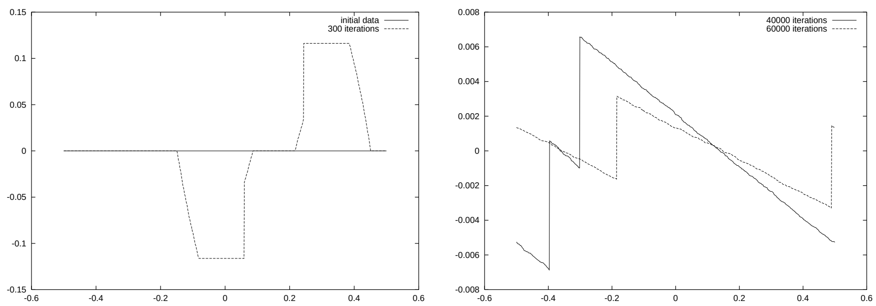

FIG. 3.23 – *Classical Riemann solution (v component)*

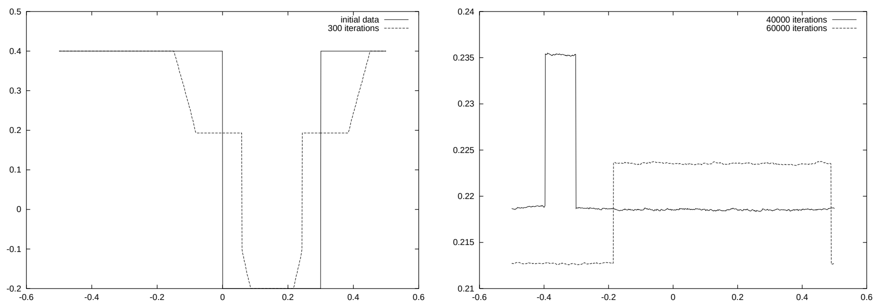

FIG. 3.24 – *Classical Riemann solution (w component)*

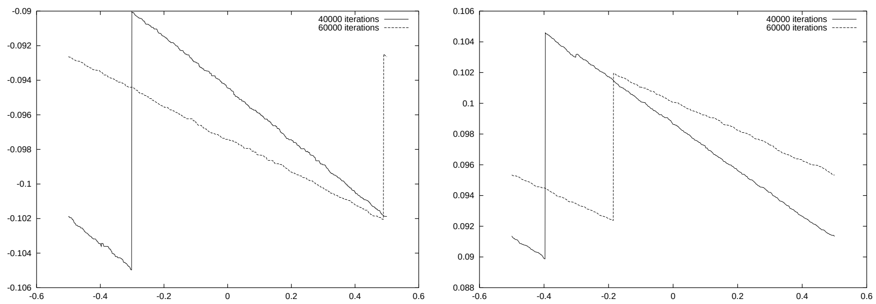

FIG. 3.25 – *Classical Riemann solution (Linearized Riemann invariants)*

Second, we choose $x_0 = -0.3.$ and $x_1 = -0.3 + 2/3$, so that the averages of v_0 and w_0 both equal 0. Figures 3.26 and 3.27 show the components v and w, respectively.

The *Riemann invariants* linearized near 0, that is,

$$v - \sqrt{\sigma'(0)}\, w \quad \text{and} \quad v + \sqrt{\sigma'(0)}\, w,$$

exhibit a *double N-wave pattern;* see Figure 3.28. We recall that the same behavior on the conservative variable was observed in the scalar case. (Compare with Figures 3.13, 3.14 and 3.17.)

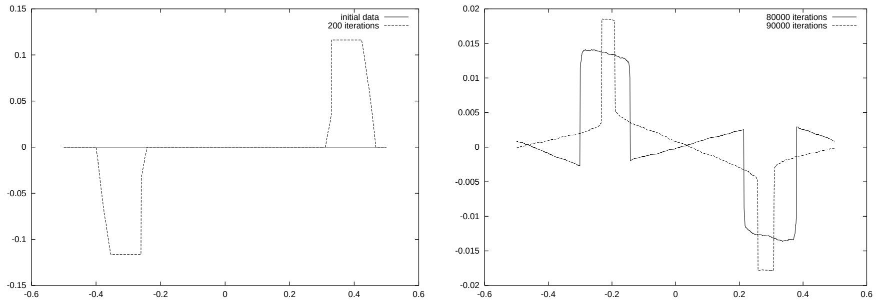

FIG. 3.26 – *Classical Riemann solution (v component)*

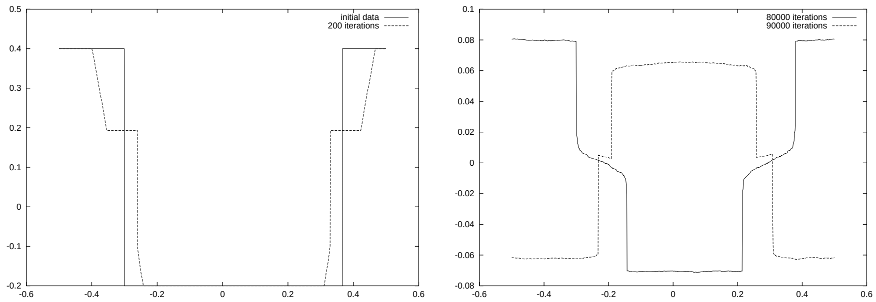

FIG. 3.27 – *Classical Riemann solution (w component)*

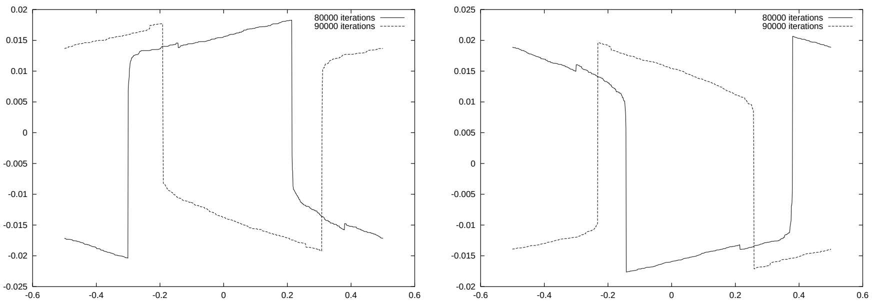

FIG. 3.28 – *Classical Riemann solution (Linearized Riemann invariants)*

• Figures 3.29-3.34: *The nonclassical case.* We now study the nonclassical value $\beta = 3/4$ together with the following periodic initial data

$$(v_0(x), w_0(x)) = \begin{cases} (0.1, 0.4), & x < x_0, \\ (0, -0.2), & x_0 < x < x_1, \\ (0.1, 0.4), & x > x_1. \end{cases}$$

Figures 3.29, 3.30, and 3.31 correspond to the choice $x_0 = 0$ and $x_1 = 3$ (so that the average of w_0 is 0.22), while Figures 3.32, 3.33, and 3.34 show the case $x_0 = -0.3$ and $x_1 = -0.3 - 2/3$ for which the average of w_0 equals zero. The same asymptotic behaviors as in the classical case are observed for the linearized Riemann invariants, that is, *standard N-waves* (Figure 3.31) and *double N-waves* (Figure 3.34), depending on the average of w_0.

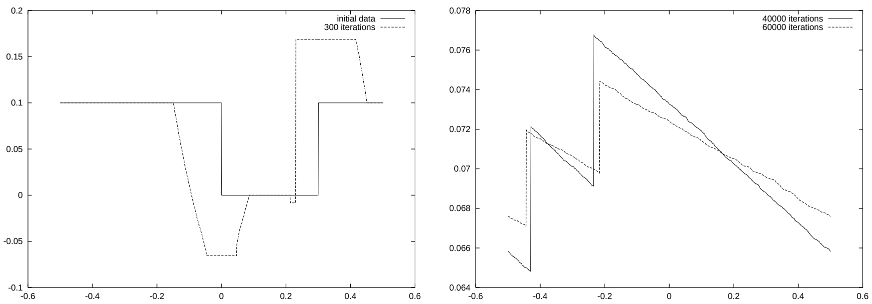

FIG. 3.29 – *Nonclassical Riemann solution (v component)*

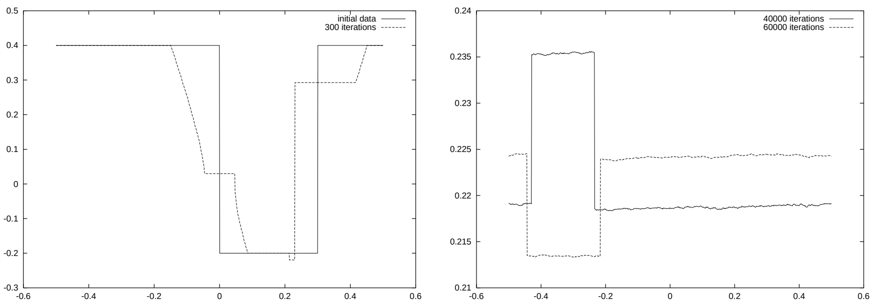

FIG. 3.30 – *Nonclassical Riemann solution (w component)*

• Figures 3.35-3.40: *The maximal nonclassical case.* Here we investigate the maximal choice $\beta = 1$, with the following periodic initial data:

$$(v_0(x), w_0(x)) = \begin{cases} (-0.3, 0.4), & x < -0.3, \\ (0, -0.2), & -0.3 < x < -0.3 + 2/3, \\ (-0.3, 0.4), & x > -0.3 + 2/3. \end{cases}$$

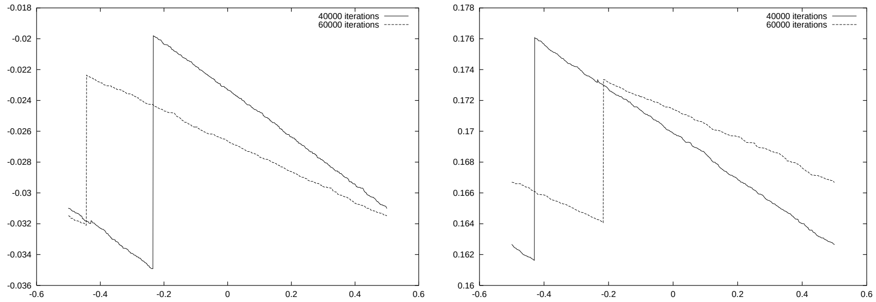

FIG. 3.31 – *Nonclassical Riemann solution (Linearized Riemann invariants)*

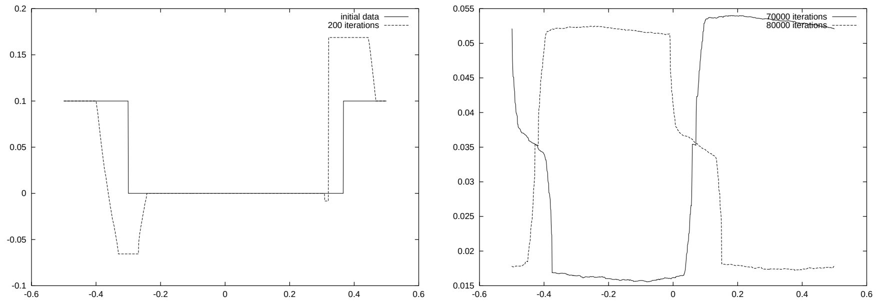

FIG. 3.32 – *Nonclassical Riemann solution (v component)*

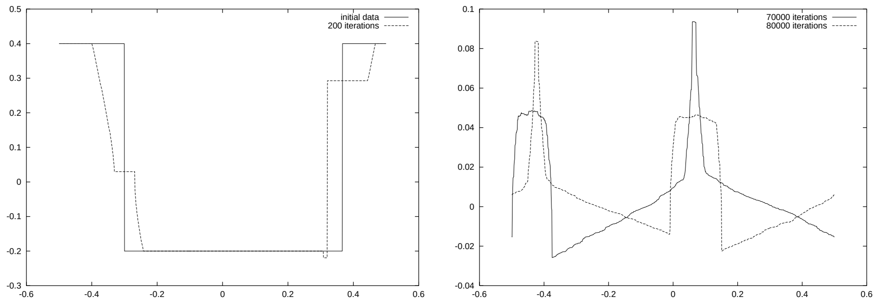

FIG. 3.33 – *Nonclassical Riemann solution (w component)*

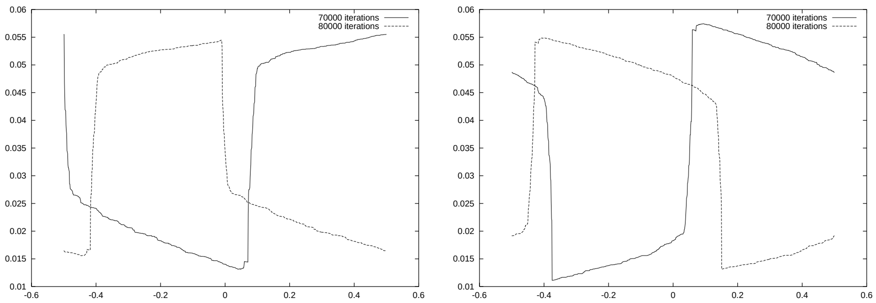

FIG. 3.34 – *Nonclassical Riemann solution (Linearized Riemann invariants)*

Here, the average of the component w equals zero. Figure 3.35 shows the component w after various numbers of iteration. For large times, we observe (as in the scalar case) that the solution tends to a piecewise constant function made of two phase transitions satisfying the prescribed kinetic relation. Since $\beta = 1$, they have the same propagation speed. Observe also that the number of phase transitions is *equal* to the one of initial data.

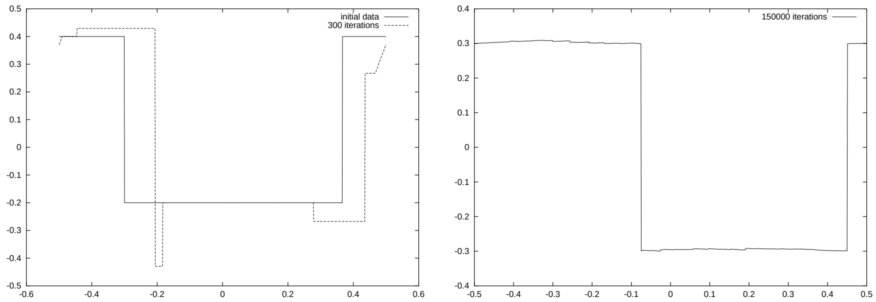

FIG. 3.35 – *Maximal nonclassical Riemann solution (w component)*

It is worth pointing out that another qualitative behavior can be observed with the maximal nonclassical Riemann solver. Indeed, if we consider the periodic initial data

$$(v_0(x), w_0(x)) = \begin{cases} (0, 0.4), & x < -0.3, \\ (0, -0.2), & -0.3 < x < -0.3 + 2/3, \\ (0, 0.4), & x > -0.3 + 2/3, \end{cases}$$

(the average of w_0 is 0 as well as the average of v_0), we observe now a *double N-wave pattern* on the linearized Riemann invariants, and for large times, the solution does not seem to converge to a solution made of phase transitions with equal propagation speeds. Asymptotically, the solution does contain two phase transitions, that is, exactly the *same* number as there was in the initial data.

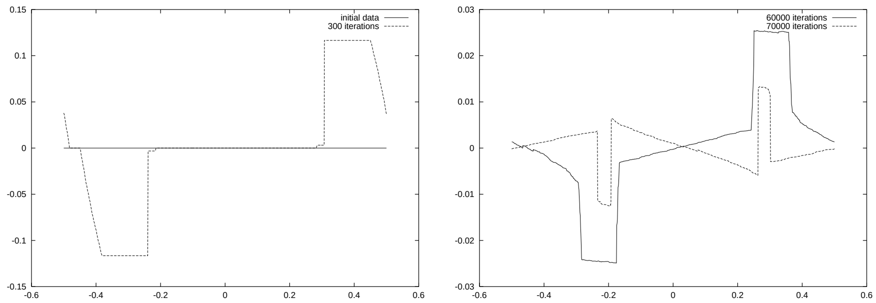

FIG. 3.36 – *Maximal nonclassical Riemann solution (v component)*

We give another test of interest which demonstrates that the number of phase transitions may be asymptotically be *larger* than the one in the initial data. Consider

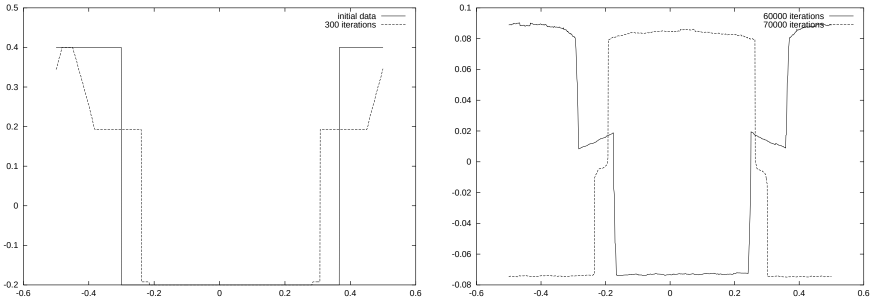

FIG. 3.37 – *Maximal nonclassical Riemann solution (w component)*

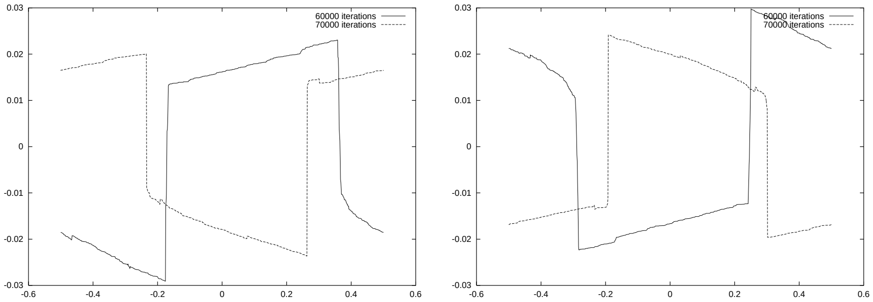

FIG. 3.38 – *Maximal nonclassical Riemann solution (Linearized Riemann invariants)*

the periodic initial data

$$(v_0(x), w_0(x)) = \begin{cases} (-0.3, 0.4), & x < -0.3, \\ (0.15, -0.2), & -0.3 < x < -0.3 + 2/3, \\ (-0.3, 0.4), & x > -0.3 + 2/3. \end{cases}$$

We plotted the component w of the solution on Figure 3.39. For large times, we observe a solution made of *four* phase transitions with coinciding propagation speeds.

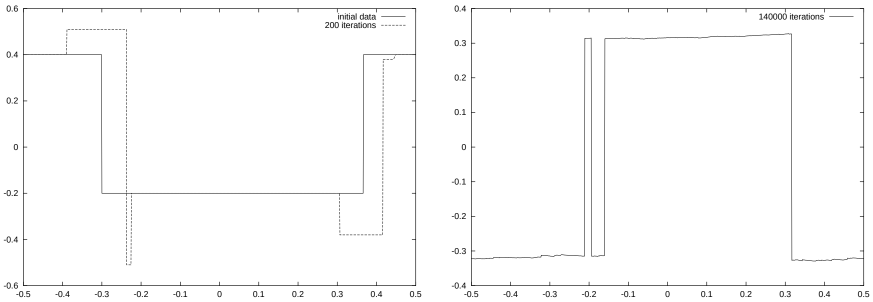

FIG. 3.39 – *Increasing the number of phase transitions (w component)*

To conclude this section, consider a periodic initial data made of four phase transitions, precisely

$$(v_0(x), w_0(x)) = \begin{cases} (0.1, 0.4), & x < -0.4, \\ (0.2, -0.3), & -0.4 < x < -0.1, \\ (0., 0.4), & -0.1 < x < 0.1, \\ (0, -0.2), & 0.1 < x < 0.3, \\ (0.1, 0.4), & x > 0.3. \end{cases}$$

We plotted the component w of the numerical solution on Figure 3.40. Observe that, here, none of the averages of v_0 or w_0 is zero. For sufficiently large times, we obtain a solution made of two phase transitions (propagating with the same speed), so that the number of transitions has decreased with respect to the one in the initial data.

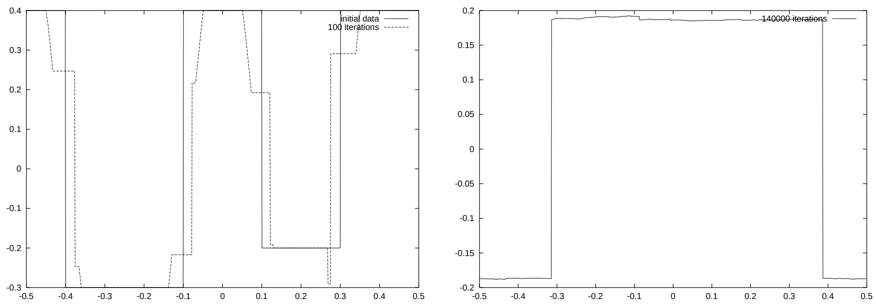

FIG. 3.40 – *Initial data made of four phase transitions (w component)*

Test 8 : Mesh refinements

Consider the initial data

$$(v_0(x), w_0(x)) = \begin{cases} (1, 3), & x < 0, \\ (0.2, -4), & x > 0. \end{cases}$$

We plot the numerical solution for several mesh lengths, at the time $t = 0.06$ and for $\beta = 2/3$. This test illustrates that the random choice method converges very sharply to the exact nonclassical solution of the problem under consideration.

3.4 Conclusions

In this paper, we have studied two hyperbolic models giving rise to nonclassical undercompressive shock waves, namely the scalar conservation laws and the model of elastodynamics when the flux is a cubic function. We have investigated the stability and time-asymptotic properties of classical and nonclassical entropy solutions.

(1) We have demonstrated that Glimm's scheme converges to exact solutions, even when the classical Riemann solver is replaced with a nonclassical Riemann solver.

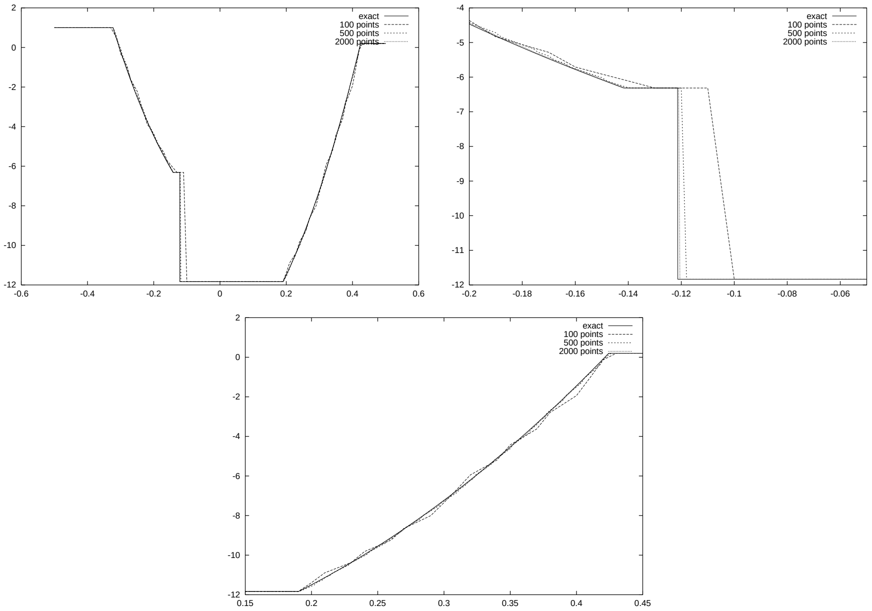

FIG. 3.41 – *System case: convergence (global v-component and zooms)*

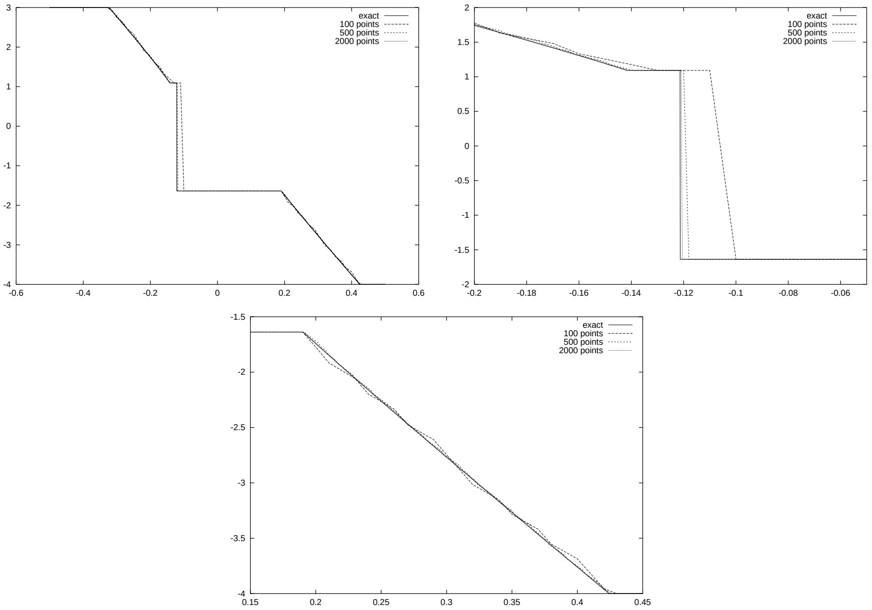

FIG. 3.42 – *System case: convergence (global w-component and zooms)*

(2) It is well-known that for classical entropy solutions the total variation is a non-increasing functional for scalar conservation laws, and, for systems, may increase only by an amount of the order of the incoming wave strength. This is no longer true for nonclassical solutions. We have observed that, under small perturbations, classical shock waves may be *split into a nonclassical shock and a classical one,* which is the reason why the *total variation of nonclassical solutions may increase drastically* as the solution evolves in time.

(3) We have studied the time-asymptotic behavior of periodic solutions. We found that any periodic solution asymptotically converges to a constant state and, more precisely, approaches a well-known N*-wave pattern* when the average of the initial data is non-zero but approaches a *"double* N*-wave pattern"* if this average equals zero. In the latter, nonclassical double N-waves contain two interfaces propagating with a speed fullfiling the Rankine-Hugoiniot relation and the kinetic relation. These conclusions hold for the conservative variable in the scalar case (Section 3.2) and for the linearized Riemann invariants for the system (Section 3.3). It would be interesting to determine this pattern analytically, but this seems to be very chalenging. It is conceivable that the existence of “double N-wave pattern is typical of classical and nonclassical solutions of general hyperbolic systems which fail to have globally genuinely nonlinear characteristic fields.

(4) Special attention was devoted to the maximal kinetic function, which allows us to exhibit still another interestig behavior of nonclassical entropy solutions. Generally speaking, the numerical solution converges for large times to an oscillating pattern involving only two constant values and a finite number of transitions propagating with the same speed. In addition, this number may decrease as well as increase in time.

A follow-up paper [27] will investigate to which extend our conclusions remain valid for the hyperbolic-elliptic version of (3.13). Additional difficulties arise in this context, for instance the lack of continuous dependence and uniqueness of the nonclassical solver (see [96]), which we will have to address from the numerical standpoint.

To close this paper, we emphasize that Glimm's compare favorably with numerical methods for computing nonclassical shock waves. In particular, by taking into account diffusive and dispersive terms directly within a finite difference scheme, it is possible to compute nonclassical shock waves with arbitary accuracy and to approach a prescribe kinetic relation generated by a zero diffusion-dispersion limit. See [64], [94], [25], [24], [93]. However the accuracy deteriorates with shocks with large strength and with large-time computations.

In contrast, Glimm's scheme

• converges to the correct solution satisfying the prescribed kinetic relation for all nonclassical shock waves, even with arbitrary strength,

• is very flexible and encompass arbitary kinetic functions, which need not be generated by a specific diffusive-dispersive mechanism, but may be determined by experiments (for instance)

• and allows one to determine large-time asymptotics of nonclassical solutions.